

Effect of wavelength on *in vivo* images of the human cone mosaic

Stacey S. Choi,* Nathan Doble,[†] and Julianna Lin

Center for Visual Science, University of Rochester, Rochester, New York 14627

Julian Christou

Center for Adaptive Optics, University of California, Santa Cruz, California 95064

David R. Williams

Center for Visual Science, University of Rochester, Rochester, New York 14627

Received November 19, 2004; revised manuscript received March 25, 2005; accepted April 21, 2005

In images of the human fundus, the fraction of the total returning light that comes from the choroidal layers behind the retina increases with wavelength [Appl. Opt. **28**, 1061 (1989); Vision Res. **36**, 2229 (1996)]. There is also evidence that light originating behind the receptors is not coupled into the receptor waveguides en route to the pupil [S. A. Burns *et al.*, *Noninvasive Assessment of the Visual System*, Vol. 11 of 1997 Trends in Optics and Photonics Series, D. Yager, ed. (Optical Society of America, 1997), p. a1; Invest. Ophthalmol. Visual Sci. **38**, 1657 (1997)]. These observations imply that the contrast of images of the cone mosaic should be greatly reduced with increasing wavelength. This hypothesis was tested by imaging the light distributions in both the planes of the photoreceptors and the pupil at three wavelengths, 550, 650, and 750 nm, with the Rochester adaptive optics ophthalmoscope. Surprisingly, the contrast of the retinal images varied only slightly with wavelength. Furthermore, the ratio of the receptorally guided component to the total reflected light measured in the pupil plane was found to be similar at each wavelength, suggesting that, throughout this wavelength range, the scattered light from the deeper layers in the retina is guided through the receptors on its return path to the pupil. © 2005 Optical Society of America

OCIS codes: 330.7310, 330.5370, 330.6130, 010.1080, 330.5310.

1. INTRODUCTION

The light that returns from the fundus in ophthalmoscopy is reflected from many layers in the retina, pigment epithelium, and choroid. Models that predict the overall spectral reflectance of the fundus in terms of the spectral properties of the ocular pigments allow inferences about the relative contribution of different layers. For example, the reflectance of human retina increases steeply with increasing wavelength owing largely to the decrease in absorption by melanin and blood.¹⁻⁴ The decline in the melanin and blood absorption allows infrared light to penetrate more deeply into the choroid. Therefore, not only does the total reflectance increase with wavelength, but there is also an increase in the fraction of light in the fundus image reflected from the deeper layers. Elsner *et al.*⁵ capitalized on this fact, using infrared light in scanning laser ophthalmoscopy to reveal choroidal structures that are difficult to image in visible light. For the same reason, the longer excitation wavelength for indocyanine green makes this dye superior to fluorescein in revealing deeper choroidal structures.⁶⁻⁸ Models of fundus reflectance suggest that the fraction of the total light returning through the pupil that comes from the deep layers behind the photoreceptors increases approximately eightfold from the middle of the visible spectrum (550 nm) into the near infrared (750 nm), whereas the relative contribution

from photoreceptors is thought to decrease accordingly by approximately threefold.^{2,3}

In addition to the spectral signatures of different pigments in the fundus, the distribution of the returning light in the pupil plane contains information about the relative contribution of different layers to the fundus reflectance.⁹⁻¹⁴ The light that enters the receptors and remains confined in them on reflection back toward the pupil will be distributed in the pupil plane in accordance with the antennae properties of the receptors.^{3,14} Each photoreceptor guides light toward a common point near the center of the pupil,^{15,16} resulting in a roughly Gaussian-shaped light distribution. The light distribution in the pupil also contains a pedestal that is thought to arise from returning light that has not been guided by the receptors.¹⁰ For example, the light returning from the anterior layers of the retina should fill the pupil uniformly because it has not passed through the cone waveguides. The distribution of light in the pupil returning from layers posterior to the photoreceptors is less certain. If this light couples into the receptors on the return pass, then one would expect this light to contribute to the directional component of the pupil plane image. However, if cones are inefficient at collecting light originating from behind the retina, then this light will contribute mainly to the pedestal.

There is little published data to allow us to decide between these hypotheses, though the prevailing view is that light reflected from deeper layers is not directional.^{11,17,18} Brindley and Rushton¹⁹ concluded that cones are relatively unexcitable from behind. They made observations of the relative brightness of lights incident on the retina in the normal fashion and lights introduced to the retina near the sclera. It is difficult to interpret their results because the actual flux density at the photoreceptors produced by transscleral illumination was not measured directly. Prieto *et al.*¹¹ and Burns *et al.*^{12,17} investigated the angular tuning of the light generated by fluorescence in the retinal pigment epithelium (RPE). They showed that the distribution of autofluorescence from lipofuscin is nondirectional, giving rise to a uniform light distribution at the pupil plane. This suggests that light arising from autofluorescence in layers behind the retina is not guided by photoreceptors.

These previous findings taken together predict that the contrast of *in vivo* images of the cone mosaic will decrease with increasing wavelength owing to the relative increase in the component reflected from the deeper layers, which is expected to be nondirectional. The ability to image the cone mosaic with a high-resolution fundus camera equipped with adaptive optics^{20,21} (AO) allows a direct test of this hypothesis. Contrary to expectation, the contrast of images of the cone mosaic declines only slightly with increasing wavelength.

2. METHODS

A. Subjects

Three subjects between the ages of 20 and 26 yr. with healthy eyes were recruited for the study. Two of the three subjects (DG and EM) were emmetropic, and one subject (JT) was mildly myopic (−2.50 diopters). In this case, the refractive error was corrected with a trial lens. After written consent was obtained in accordance with the Declaration of Helsinki, the pupil was dilated with one drop of 1% tropicamide and one drop of 2.5% phenylephrine prior to data collection. A dental impression was used to stabilize the subject's head.

B. Procedure

The Rochester AO ophthalmoscope^{20,21} was used to take images in both retinal and pupil planes at three different wavelengths, 550, 650, and 750 nm. In each case, the full width at half-maximum (FWHM) of the spectral interference filter used was 25 nm. Acquisition of the pupil plane images required the insertion of an extra achromatic doublet lens (focal length = +40 cm) in the science camera arm to make the normally retinal conjugate CCD camera conjugate to the pupil plane. The subject was instructed to observe the 1 deg, temporal fixation mark while flashlamp pulses of 4 ms duration were delivered to the eye.

The entrance pupil for the flash had a diameter of 2 mm; its small size was chosen to maximize the fraction of incident light guided into the photoreceptors. All images were obtained through a 6 mm exit pupil that remained centered on the subjects' pupils throughout the experiment. For the 2 mm entrance pupil, the flashlamp

pulses had energies of 0.279, 0.195, and 0.122 mJ for the 550, 650, and 750 nm wavelengths, respectively.

The position of the entrance pupil was translated both vertically and horizontally in 1 mm increments until the best pupil image was observed on the CCD camera. The best image was defined as the position in which the intensity of the directional component was largest without the problematic first Purkinje image due to the corneal reflection.

To keep image noise constant across wavelength, the amount of reflected light captured by the imaging camera was equalized for all wavelengths with neutral-density filters in the flashlamp arm and adjustments of the flashlamp voltage. To increase the amount of light returning from the eye and to eliminate wavelength-dependent variations in photopigment transmittance, the photopigment in the retinal location to be imaged was first bleached with a 10 s exposure of 550 nm light at 37×10^6 td-s. This exposure duration and intensity bleached 98% of the photopigment.²²

Following the bleach, five images of the same wavelength were taken with approximately 5 s between images. The photopigment was then bleached again, and an additional five images were taken. The wavelength was randomly varied between each set of five images until 30–40 images were collected per wavelength. For each of the three wavelengths, the seven best images (e.g., those without debris in the tear film on the cornea) were registered and averaged.

After the pupil plane images were acquired, images were taken of the photoreceptor mosaic under the same conditions and with the same procedure, with one exception: The lens (focal length = +40 cm) was removed from the imaging pathway to make the CCD camera conjugate with the plane of the photoreceptors instead of the pupil. The field on the retina subtended 1 deg. Minor refocusing was required to maximize the contrast of the images of cones at each wavelength. The resolution of the CCD camera in the retinal imaging plane for each of the three subjects, DG, EM, and JT, was 0.59, 0.60, and 0.62 $\mu\text{m}/\text{pixel}$, respectively, corresponding to approximately five to seven pixels per cone. Both the pupil and retinal plane images for a particular subject were taken in the same experimental session.

3. RESULTS

A. Analysis of the Pupil Plane Images

The intensity distribution of the pupil plane image consists of a guided component directed toward the center of the pupil, which sits on a pedestal representing the diffuse, scattered light. This distribution is illustrated schematically in Fig. 1A. Following Burns *et al.*,²³ a Gaussian function was fitted with a least-squares procedure to the light distribution, L_{PUPIL} , recorded in the 6 mm exit pupil:

$$L_{\text{PUPIL}}(r) = B + A \times 10^{-\rho r^2}, \quad (1)$$

where A is the amplitude of the guided component assumed to come from the cones, ρ (in inverse millimeters squared) is the space constant of the Gaussian profile, B

is the amplitude of the diffuse component or uniform pedestal beneath the guided component, and r (in millimeters) is the distance from the peak of the intensity distribution.

The volumes underneath the guided light distribution, G_p , and the diffuse component, D_p , were calculated for each of the three wavelengths. To assess the contribution from the cones to the total reflected light, the ratio of the volume of the guided component to the total volume within the pupil was computed. This is referred to here as the guided fraction of the pupil image, C_p :

$$C_p = \frac{G_p}{G_p + D_p}. \quad (2)$$

Figure 2 shows a cross section through the pupil image of one subject, EM, at each of the three wavelengths. Data points from the original image are shown as dots. The guided component has been fitted with the Gaussian function²³ described in Eq. (1) and is shown as a solid curve.

It is clear from Fig. 2 that the amplitude of the guided component, A , decreased with increasing wavelength, whereas the breadth of the Gaussian function increased. This same pattern was observed in all three subjects.

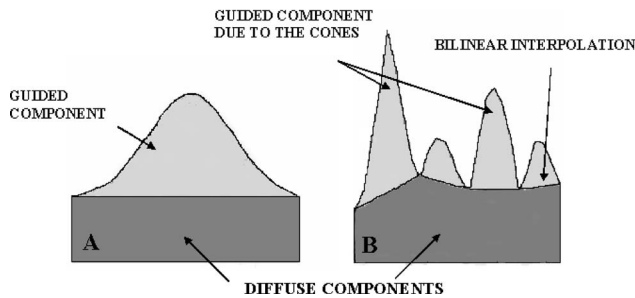


Fig. 1. Schematic cross sections of the diffuse and guided components for the pupil and retinal planes. A, Pupil plane. The guided component (light gray) has a Gaussian profile that is most often centered in the pupil aperture, and the guided component sits above the diffuse pedestal (dark gray). B, Analogous cross section in the retinal image space. The peaks correspond to the waveguided light in the cones and have a Gaussian-like distribution. The floor of the guided component was found through bilinear interpolation. The waveguided contribution lies above the diffuse light scattered from the anterior and posterior layers to the photoreceptor plane.

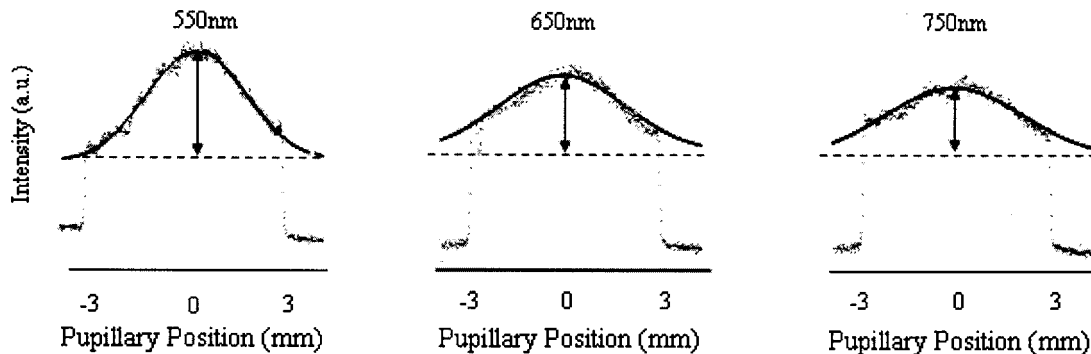


Fig. 2. Guided and diffuse components measured in the pupil plane at the three wavelengths for subject EM. The total quantum flux measured by the pupil conjugate CCD camera was equalized across wavelength. All three subjects showed the same trend of results: The amplitude and the ρ value of the guided component decrease with increasing wavelength; therefore, the overall volume of the guided fraction stays similar across wavelength. The guided fraction was fitted with a Gaussian function (solid curve) given by Eq. (1).

Therefore, when the volume of the guided component was considered, the ratio of the guided component, G_p , to the sum of the guided and diffuse components ($G_p + D_p$) remained surprisingly similar. The values for the guided fraction, C_p , across all three subjects ranged from 0.528 to 0.655, and the variation in C_p was not statistically significant, with $p > 0.05$. A summary of the ρ and C_p values calculated for all three subjects is shown in Table 1.

Figure 3A shows the total retinal reflectance for each of the imaging wavelengths as measured from the light distribution in the pupil planes for each of the three observers. To measure the reflectance, we followed the method described by Pallikaris *et al.*²⁴ The total reflectance was defined as the ratio of the irradiance at the CCD camera when a subject's retina is in the optical system to the irradiance at the CCD camera when the eye is replaced by a highly reflective (97%) mirror located in the pupil plane. The ratio of the irradiances, and hence the reflectance due to the mirror, R_M , was calculated for each combination of flashlamp voltage, neutral-density filter, and spectral interference filter used for each of the three subjects.

From Fig. 3A, it is clear that the total reflectance of the retina does increase substantially with increasing wavelength for all subjects, as expected. The observed change with longer wavelength averaged a ninefold increase, which is consistent with the values of 4 and 10–15 reported by van de Kraats *et al.*³ and Delori *et al.*,² respectively.

Figure 4A shows the guided fraction, C_p , averaged across the subjects in the pupil plane. The guided fraction ranged from 0.55 to 0.60 times the total reflectance across wavelengths in the 550–750 nm range. The variation in the guided fraction with wavelength for the pupil images was not statistically significant ($p > 0.05$). This result would not be expected unless the deeply penetrating light is coupled back into the receptors. We found no evidence that the cone fraction, C_p , varied with wavelength in any of the three subjects.

B. Analysis of the Retinal Plane Images

The intensity distribution of the retinal plane image can be likened to a two-dimensional array of spatially separated, rotationally symmetric, Gaussian-like functions that sit on top of a diffuse background, where each Gaussian-like function represents the distribution of light

exiting a single cone photoreceptor. Since the contrast of the photoreceptor mosaic is related to the strength of the modulated signal versus the background level of the image, the retinal plane images were analyzed by examining the intensities of the local maxima and the local minima in the image.

More specifically, in a procedure analogous to that described for the pupil plane images, the intensity distribution of the retinal plane image was divided into guided (modulated) and diffuse (background) components. A typical cross-sectional profile through four photoreceptors is shown schematically in Fig. 1B.

To analyze this distribution, we determined the location of the peak intensity (local maxima) corresponding to individual cone locations and the intensity at six to nine

locations around the estimated boundary of each cone (local minima). Using bilinear interpolation, a surface was created that passed through all the trough values. The volume beneath this surface was taken as the diffuse component, D_r , whereas the volume above was taken to be the total guided component, G_r . The guided fraction of the retinal image, C_r , was then given by

$$C_r = \frac{G_r}{G_r + D_r}. \quad (3)$$

C. Deconvolution of Retinal Plane Images

The receptor fraction of the retinal image is a lower bound on the light that passes through the receptors on the return pass. The diffuse component in the retinal image overestimates the amount of light that passes between receptors. Blur from diffraction at the eye's pupil as well as residual aberrations and light scatter in the eye's optics casts some of the receptor light into the troughs between cones in the image. This blur is wavelength dependent because of the dependence of diffraction on wavelength, which could confound our attempt to compare images of the retina at different wavelengths. To reduce this problem, we used deconvolution to remove the image blur caused by both diffraction and the residual aberrations in the eye that remained uncorrected by the adaptive optics (AO) system. The images were deconvolved on the basis of point-spread functions (PSFs) generated from the 60 Zernike coefficients measured by the wavefront sensor of the AO system. These coefficients were calculated for a 6 mm diameter pupil with the numbering scheme set forth in the Optical Society of America's rec-

Table 1. Summary of Pupil Plane Results for Subjects JT, EM, and DG^a

Subject	Wavelength (nm)	ρ (mm ⁻²)	C_p
JT	550	0.13	0.552
	650	0.06	0.550
	750	0.05	0.560
EM	550	0.17	0.585
	650	0.13	0.528
	750	0.02	0.655
DG	550	0.11	0.572
	650	0.06	0.572
	750	0.05	0.573

^a ρ represents the space constant of the Gaussian profile, measured in mm⁻². C_p is the guided fraction of the intensity distribution, as calculated from the pupil plane images.

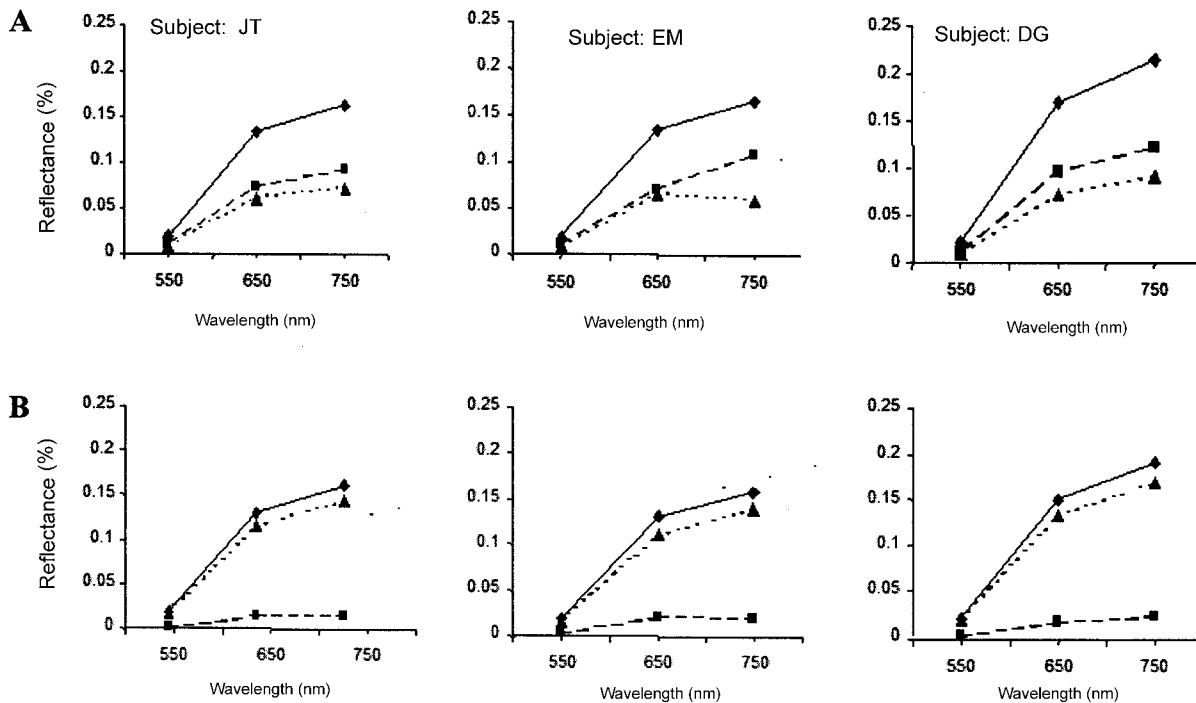


Fig. 3. A, Variation of retinal reflectance plotted as a function of wavelength for the pupil plane images. The results for all three subjects, JT, EM, and DG, are shown. Solid curves represent the total retinal reflectance, whereas dashed and dotted curves represent the guided and diffuse components of the total reflectance, respectively. B, Analogous plots of retinal reflectance plotted as a function of wavelength for the retinal images. The total reflectance values measured in both the retinal and the pupil planes agree strongly; however, the guided component is larger at the pupil plane.

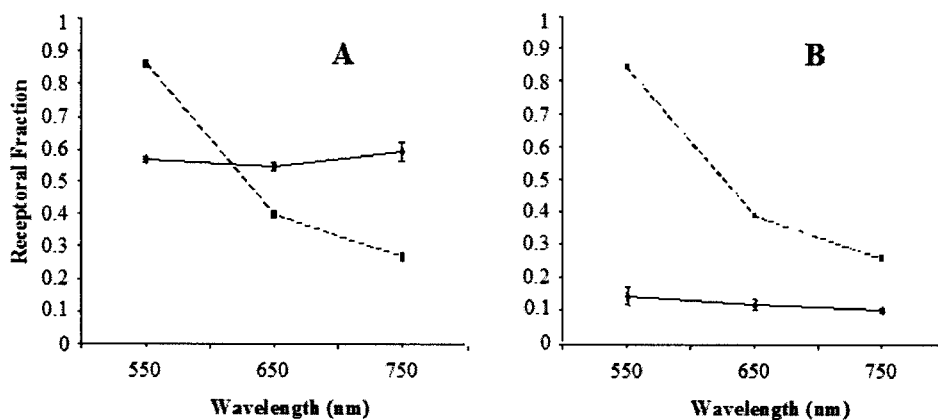


Fig. 4. A, Guided fraction, C_p , from the pupil images (i.e., irradiance from the guided component divided by the total irradiance) as a function of wavelength (solid curve). B, Analogous plot for the guided fraction, C_r , from the retinal images. For both figures the solid curves are the means of three subjects, the error bars representing one standard deviation. The dashed curves represent the prediction from the retinal reflectance model of van de Kraats *et al.*³ with the added assumption that no light reflected from layers behind the retina is coupled back into receptors. For both the retinal and the pupil plane images, the guided fraction of the total reflectance stayed essentially constant across wavelength in contrast to the predictions.

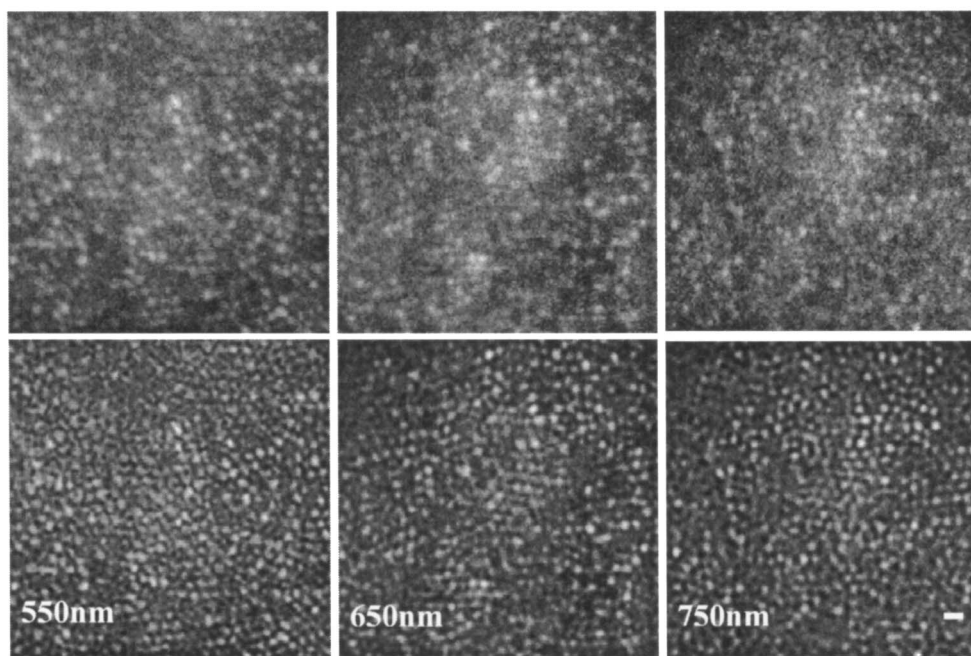


Fig. 5. Retinal plane images for subject DG at an eccentricity of 1 deg in the temporal retina. The top row shows the registered raw images for the three imaging wavelengths 550, 650, and 750 nm. The bottom row shows the same images but deconvolved using the system PSF. The scale bar corresponds to 10 μm .

ommended standards.²⁵ Each PSF was computed using the Fourier modulus squared of a complex wavefront with unit amplitude within the pupil support (6 mm) and zero outside. A multiframe iterative deconvolution technique was applied. This algorithm has been previously applied to retinal images for cone classification²⁶ and is described elsewhere.^{27,28} This algorithm permits the PSFs to also vary within external constraints while solving for a common object from a set of multiple input images. For this application, the initial PSFs were those generated from the Zernike polynomial wavefront fits, and the initial object was the coadded, registered raw data. Although deconvolution reduces the effect of the eye's optics, it does not correct for light scatter, which is not measured by

Shack–Hartmann wavefront sensing. For this reason, the cone fraction calculated here will underestimate the true cone fraction, a point that is returned to in the discussion.

Figure 5 shows retinal images taken at three different wavelengths for subject DG. The top row shows the registered mean of the best images collected from the AO system, and the bottom row shows the results of the same images deconvolved with the system PSF. The main result is that, though the deconvolved images have higher contrast than the raw images, in each case, there is little effect of wavelength on image contrast. For example, the modulation transfer function (MTF) for a 6 mm pupil is

on average only 18% higher at 550 nm than at 750 nm, with the MTF for 650 nm lying in between.

For subject DG, the guided fraction, C_r , of the light distribution for the original set of images ranged from 0.108 to 0.138. By comparison, the guided fraction of the deconvolved images was approximately two times higher and ranged from 0.257 to 0.301. Subjects EM and JT also had similar results, with C_r values for the deconvolved images that ranged from 0.283 to 0.348 and from 0.168 to 0.209, respectively. Again, the variation of the guided fraction, C_r , with wavelength was not statistically significant, with $p > 0.05$.

Figure 3B shows the total retinal reflectance as a function of wavelength for each of the three observers as calculated from the retinal images. As in the case of the pupil images, the average total reflectance, which is the sum of the cone and diffuse values, increased with wavelength, from 0.02% at 550 nm to 0.17% at 750 nm, a factor of 8.5. This value lies between the values of 4 and 10–15 reported by van de Kraats *et al.*³ and Delori *et al.*,² respectively. Not only does the total reflectance increase with wavelength but both the cone and the diffuse component also increase.

The reflectance from the retinal images was calculated using the procedure of Pallikaris *et al.*²⁴ The reflectance is defined as the ratio of the irradiance at the imaging camera when a subject's retina is in the optical system to the irradiance at the CCD camera when the eye is replaced by a highly reflective mirror located in the pupil plane. This method for calculating the reflectance results in lower values than other studies because of our use of a mirror where the eye's pupil plane would normally reside rather than a Lambertian scatterer in the retinal plane of an artificial eye.^{2,3} We prefer the mirror method because the estimate of reflectance then captures all the light losses within the eye.

Equation (4) gives the formula relating the mirror reflectance, R_M , to that of a Lambertian surface, R_L :

$$R_L = R_M \frac{d^2}{d^2 + 4f^2}, \quad (4)$$

where d is the diameter of the exit pupil of the eye (6 mm) and f is the ocular focal length (taken to be 17 mm).

With Eq. (4), the reflectance values obtained using the method of Pallikaris *et al.*²⁴ were rescaled to that of a Lambertian scatterer. The reflectance values at each wavelength averaged across the three subjects were 0.63%, 4.55%, and 5.62% for the 550, 650, and 750 nm wavelengths, respectively. This is in agreement with previous studies that measured the eye reflectance using a Lambertian surface.^{2,3}

Figure 4B shows the guided fraction, C_r , as a function of wavelength, averaged across all three observers. The average distance between adjacent cones, χ , the guided fraction, C_r , and the ratio of the guided fraction in the retinal image to the guided fraction in the pupil image, C_r/C_p , for each subject at each wavelength are also shown in Table 2.

The fraction of the total reflectance originating from cones averaged approximately 0.126, and the variation with wavelength was not statistically significant, with p

Table 2. Summary of Retinal Plane Results for Subjects JT, EM, and DG^a

Subject	Wavelength (nm)	C_r	C_r/C_p	$\chi(\mu\text{m})$
JT	550	0.106	0.192	4.26
	650	0.106	0.193	4.26
	750	0.096	0.171	4.26
EM	550	0.198	0.338	3.72
	650	0.153	0.289	3.72
	750	0.118	0.180	3.72
DG	550	0.138	0.241	3.35
	650	0.108	0.189	3.35
	750	0.113	0.197	3.35

^a C_r is the guided fraction of the intensity distribution, as calculated from the retinal plane images. C_r/C_p is the ratio of the guided fraction calculated from the retinal plane image before deconvolution to the guided fraction calculated from the pupil plane image. Finally, χ is the average distance across wavelength between adjacent cones in the photoreceptor mosaic, measured in micrometers.

> 0.05 . Figure 4B also shows the guided fraction that would be predicted from the fundus reflectance model of van de Kraats *et al.*³ if none of the light that penetrated behind the receptors were guided back through them. In this case, the guided fraction would drop by a factor of 3, an amount that is not evident in either the raw or the deconvolved images of the cone mosaic. Collectively, our results demonstrate that the fraction of the total reflectance due to cones is roughly independent of wavelength across the 550–750 nm range.

4. DISCUSSION

The main conclusion of these experiments is that the fraction of the fundus reflectance that contains the signature of cones is independent of wavelength across the range from 550 to 750 nm. This conclusion was obtained with two different methods: analysis of the guided component of the pupil plane image as well as analysis of the cone component of the retinal image.

Though the cone fraction of the light is not wavelength dependent, the cone fraction estimated from the retinal images is about four times smaller than that estimated from the pupil plane images. One reason for this is that the retinal images, unlike the pupil plane images, are subject to blur by the eye's optics, which reduces the modulation in the image that can be directly attributed to cones. We employed AO and deconvolution to reduce this modulation loss, but our measurements are still subject to scatter in the retina and the eye's optics. Miller *et al.*²⁹ estimated that the contrast of the cone mosaic is quite high in visible light (555 nm), approaching 100% in simulation, implying that the spaces between cones are quite dark in the retinal image. The study used a small field to illuminate the retina (6.8 arc min), which tends to reduce blur due to light scatter. The cone fraction estimated from the pupil images is likely to be an underestimate of the light that is guided through the receptors. For example, rods account for approximately 50% of the retinal area at this eccentricity,³⁰ and the light guided by them will presumably contribute to the diffuse component rather than the guided component owing to the breadth of their angular tuning.³¹

Our results are difficult to reconcile with several other lines of evidence. First, the prevailing view has been that light that penetrates deep into the fundus, such as infrared light, does not get efficiently coupled into the cones. Our result suggests that either the variation with wavelength in the depth of penetration is much less than previously thought or that deeply penetrating light does in fact get efficiently coupled into cone outer segments on the return pass. The first alternative seems unlikely given the obvious increases in the contrast of choroidal vessels observed in infrared light. The contrast has been shown to increase by about a factor of 2 as the wavelength increased from 800 to 900 nm.⁵

For reasons that are not yet clear, it seems that when the cone mosaic is backilluminated with light, the cones, rather than the spaces between them, transmit light. Earlier work by Enoch³² showed the same observation in excised retina of various animals and demonstrated that the receptors can be illuminated in both directions (i.e., from inner-to-outer-segment as well as from outer-to-inner-segment direction) to produce the same waveguided modes. These results are in accordance with Helmholtz's reciprocity theorem in optics. However, this does not seem to be the case for all sources of backillumination in living eyes (i.e., intact retina). Burns *et al.*¹⁷ have provided compelling evidence that at least one source of light originating from behind the receptors, autofluorescence by lipofuscin in the RPE, is not guided back toward the pupil and diffusely fills the pupil instead. An imaging densitometer was used to measure the distribution of light emerging from the pupil in that study. The uniform distribution of intensity for autofluorescence was shown to hold for both longer- and shorter-wavelength light and also for near the peak of the Stiles–Crawford function and far from the peak. Since lipofuscin is located in the scleral side of the retinal pigment epithelium, it makes sense that this light could be much less efficient in launching guided modes at the outer segment tip. More work will be required to clarify why lipofuscin autofluorescence is not guided back through receptors, whereas long-wavelength light that also originates from layers behind the receptors is.

Several models have been proposed over the past decades to describe the pathways of light through the retina in both directions. Some authors^{9,14} have assumed that the light waveguided by photoreceptors on its return path arises from scattering by the melanin granules close to the tips of the outer segments. An alternative model was proposed by van de Kraats *et al.*³ stating that the origin of reflected light through photoreceptors is from the stack of discs within the outer segments and the flat background represents diffusely reflected and backscattered light, which originates from various layers in the retina but in particular from the choroid. The contribution of the receptor layer to the reflected light from the retina was shown to decrease with increase in wavelength as shown in Fig. 4. However, in our study, the cone fraction was found to be constant across wavelength, 550–750 nm. We do not know enough about the passage of light through cones to exclude the possibility that light of different wavelengths returning from the choroid can enter at other points besides the tip of the outer segment.

The directional properties of cones, assessed with ρ (ρ) values of our study, agree with those of previous studies.^{13,32} We found that the ρ value decreases (i.e., the curve broadens) with increasing wavelength. Marcos *et al.*^{13,33} also showed the same trend of ρ -value change with wavelength. The ρ values in their study decreased from 0.17 at 543 nm to 0.12 at 670 nm, whereas our data changed from 0.14 at 550 nm to 0.08 at 650 nm (these are the mean values across three subjects).

Recent work by Zagers and van Norren³⁴ measured the amplitude of the directional component of the bleached fundus reflectance as a function of wavelength. They argued that the photoreceptors are spectrally neutral reflectors, which is in conflict with the conclusions of the present study. They made the assumption that if the integrated flux (i.e., the volume of the distribution of reflectance in the pupil plane) were to be spectrally neutral, the amplitude would decrease with increasing wavelength. Their results showed a slight decrease in amplitude with wavelength (from 1.71% at 400 nm to 1% at 650 nm). These amplitude values were then expressed as optical density values by taking minus the logarithm to base 10, which made the variation between the wavelengths minimal. On the other hand, both our pupil and retinal imaging results showed an increase in the total light from receptors with wavelengths of 550–750 nm. Zagers and van Norren³⁴ were unable to obtain reliable data beyond 650 nm, and it may be that part of the discrepancy is due to the fact that different ranges of wavelengths were involved in the two studies.

More recently, it has been demonstrated that it is possible to obtain high-contrast images of the cone mosaic at 900 nm using the Rochester AO ophthalmoscope.³⁵ This provides additional qualitative support for our conclusion that cone contrast is remarkably well preserved with increasing wavelength. The invariance in the contrast of the cone mosaic with wavelength suggests that light that penetrates behind the retina and is scattered back toward the pupil has a preferred path through the outer segments of photoreceptors.

It is tempting to think that the visual system has evolved to increase the photoreceptor quantum catch, much as it has been argued that the cat's tapetum increases its sensitivity in the dark.^{36,37} However, owing to the high absorption of light by melanin in the visible portion of the spectrum, the amount of light making a second pass through the receptor is so small relative to the first pass that there would seem to be little advantage conferred by such a mechanism.

5. CONCLUSION

In fundus imaging, light that returns to the pupil from the deeper retinal layers must pass through the photoreceptor layer. We show that most of that light is coupled back into the photoreceptors and is guided toward the pupil. One practical consequence of this result for vision research is that in high-resolution retinal imaging the photoreceptor mosaic retains its contrast into the near infrared. This allows the noninvasive investigation of the normal and diseased cone mosaics *in vivo* with imaging wavelengths in the near infrared, which are more com-

portable and less hazardous to the patient.

ACKNOWLEDGMENTS

We thank Gang Pan for his help with the data analysis, all the subjects who have participated in this study, and Joseph Carroll for imaging at 900 nm. This work was supported in part by the National Science Foundation through the Center for Adaptive Optics, managed by the University of California at Santa Cruz, and through National Eye Institute grants, EY04367 and EY01319, and a grant from the Steinbach Foundation.

Direct all correspondence to Stacey Choi by e-mail at sschoi@ucdavis.edu.

*Currently at the Department of Ophthalmology, University of California, Davis, Davis, California 95817.

†Currently at Iris AO, Inc., 2680 Bancroft Way, Berkeley, California 94704.

REFERENCES

- D. van Norren and L. F. Tiemeijer, "Spectral reflectance of the human eye," *Vision Res.* **26**, 313–320 (1986).
- F. C. Delori and K. P. Pflibsen, "Spectral reflectance of the human ocular fundus," *Appl. Opt.* **28**, 1061–1077 (1989).
- J. van de Kraats, T. T. J. M. Berendschot, and D. van Norren, "The pathways of light measured in fundus reflectometry," *Vision Res.* **36**, 2229–2247 (1996).
- N. P. A. Zagers, J. van de Kraats, T. T. J. M. Berendschot, and D. van Norren, "Simultaneous measurement of foveal spectral reflectance and cone-photoreceptor directionality," *Appl. Opt.* **41**, 4686–4696 (2002).
- A. E. Elsner, S. A. Burns, J. J. Weiter, and F. C. Delori, "Infrared imaging of sub-retinal structures in the human ocular fundus," *Vision Res.* **36**, 191–205 (1996).
- A. E. Elsner, J. J. Weiter, G. Staurenghi, S. A. Burns, K. J. Wald, S. Wolf, and S. M. Buzney, "Use of infrared imaging in interpreting indocyanine green angiography," *Invest. Ophthalmol. Visual Sci.* **34**, 1135 (1993).
- S. Wolf, K. J. Wald, A. E. Elsner, and G. Staurenghi, "Indocyanine green choroidal videoangiography—a comparison of imaging analysis with the scanning laser ophthalmoscope and the fundus camera," *Retina* **13**, 266–269 (1993).
- K. J. Wald, A. E. Elsner, S. Wolf, G. Staurenghi, and J. J. Weiter, "Indocyanine green videoangiography for the imaging of choroidal neovascularization associated with macular degeneration," *Int. Ophthalmol. Clin.* **34**, 311–325 (1994).
- G. J. van Blokland, "Directionality and alignment of the foveal receptors, assessed with light scattered from the human fundus *in-vivo*," *Vision Res.* **26**, 495–500 (1986).
- S. A. Burns, S. Wu, F. C. Delori, and A. Elsner, "Direct measurement of human-cone-photoreceptor alignment," *J. Opt. Soc. Am. A* **12**, 2329–2338 (1995).
- P. M. Prieto, J. S. McLellan, and S. A. Burns, "Investigating the light absorption in a single pass through the photoreceptor layer by means of the lipofuscin fluorescence," *Vision Res.* **45**, 1957–1965 (2005).
- S. A. Burns, J. C. He, F. C. Delori, and S. Marcos, "Do the cones see light scattered from the deep retinal layers?" in *Noninvasive Assessment of the Visual System*, Vol. 11 of 1997 Trends in Optics and Photonics Series, D. Yager, ed. (Optical Society of America, 1997), pp. a1–a4.
- S. Marcos and S. A. Burns, "Cone spacing and waveguide properties from cone directionality measurements," *J. Opt. Soc. Am. A* **16**, 995–1004 (1999).
- J. M. Gorrand and F. C. Delori, "A reflectometric technique for assessing photoreceptor alignment," *Vision Res.* **35**, 999–1010 (1995).
- A. M. Laties and J. M. Enoch, "An analysis of retinal receptor orientation. I. Angular relationship of neighboring photoreceptors," *Invest. Ophthalmol.* **10**, 69–77 (1971).
- A. Roorda and D. R. Williams, "Optical properties of individual human cones," *J. Vision* **2**, 404–412 (2002).
- S. A. Burns, F. C. Delori, and J. C. He, "Back-illuminating the cones: Is the light from the RPE guided?" *Invest. Ophthalmol. Visual Sci.* **38**, 57, Part 1 (1997).
- F. C. Delori, D. G. Goger, B. R. Hammond, D. M. Snodderly, and S. A. Burns, "Foveal lipofuscin and macular pigment," *Invest. Ophthalmol. Visual Sci.* **38**, 1657, Part 1 (1997).
- G. S. Brindley and W. A. H. Rushton, "The color of monochromatic light when passed into the human retina from behind," *J. Physiol. (London)* **147**, 204–208 (1959).
- J. Liang, D. R. Williams, and D. T. Miller, "Supernormal vision and high-resolution retinal imaging through adaptive optics," *J. Opt. Soc. Am. A* **14**, 2884–2892 (1997).
- H. Hofer, L. Chen, G. Y. Yoon, B. Singer, Y. Yamauchi, and D. R. Williams, "Improvement in retinal image quality with dynamic correction of the eye's aberrations," *Opt. Express* **8**, 631–642 (2001).
- M. Hollins and M. Alpern, "Dark adaptation and visual pigment regeneration in human cones," *J. Gen. Physiol.* **62**, 430–447 (1973).
- S. A. Burns, S. Wu, J. C. He, and A. E. Elsner, "Variation in photoreceptor directionality across the central retina," *J. Opt. Soc. Am. A* **14**, 2033–2040 (1997).
- A. Pallikaris, D. R. Williams, and H. Hofer, "The reflectance of single cones in the living human eye," *Invest. Ophthalmol. Visual Sci.* **44**, 4580–4592 (2003).
- L. N. Thibos, R. A. Applegate, J. T. Schwiegerling, and R. Webb, "Standards for reporting the optical aberrations of eyes," *J. Refract. Surg.* **18**, S652–S660 (2002).
- J. C. Christou, A. Roorda, and D. R. Williams, "Deconvolution of adaptive optics retinal images," *J. Opt. Soc. Am. A* **21**, 1393–1401 (2004).
- J. C. Christou, D. Bonaccini, N. Ageorges, and F. Marchis, "Myopic deconvolution of adaptive optics images," *ESO Messenger* **97**, 14–22 (1999).
- S. M. Jefferies and J. C. Christou, "Restoration of astronomical images by iterative blind deconvolution," *Astrophys. J.* **415**, 862–874 (1993).
- D. T. Miller, D. R. Williams, G. M. Morris, and J. Liang, "Images of cone photoreceptors in living human eye," *Vision Res.* **36**, 1067–1079 (1996).
- C. A. Curcio, K. R. Sloan, R. E. Kalina, and A. E. Hendrickson, "Human photoreceptor topography," *J. Comp. Neurol.* **292**, 497–523 (1990).
- J. M. Enoch and F. L. Tobey, *Vertebrate Photoreceptor Optics* (Springer-Verlag, 1981).
- J. M. Enoch, "Visualization of waveguide modes in retinal receptors," *Am. J. Ophthalmol.* **51**, 1107/235–1118/246 (1961).
- S. Marcos, S. A. Burns, and J. C. He, "Model for cone directionality reflectometric measurements based on scattering," *J. Opt. Soc. Am. A* **15**, 2012–2022 (1998).
- N. P. A. Zagers and D. van Norren, "Absorption of the eye lens and macular pigment derived from the reflectance of cone photoreceptors," *J. Opt. Soc. Am. A* **21**, 2257–2268 (2004).
- J. Carroll, Center for Visual Science, University of Rochester, New York 14627 (personal communication, 2005).
- G. Walls, "The vertebrate eye and its adaptive radiation," *Bull. Cranbrook. Inst. Sci.* **19**, 785 (1942).
- R. A. Weale, "The spectral reflectivity of the cat's tapetum measured *in situ*," *J. Physiol. (London)* **119**, 30–42 (1953).